David PÁNEK[1], Václav KOTLAN[1], Ivo DOLEŽEL[2]

[1]University of West Bohemia, Pilsen, Czech Republic, [2]Academy of Sciences of the Czech Republic, Prague, Czech Republic

Optimization of Special Inductor for Induction Pre-heating

Abstract. The shape of a device for induction pre-heating of steel bodies is optimized in order to obtain its best performance. The goal is to maximize heat delivered to the place of the body that will be post-heated by laser beam, while heat produced elsewhere should be minimized. The direct problem (hard-coupled analysis of magnetic and temperature fields in the system) is solved by the finite element method. The inverse problem is solved using a special genetic algorithm with some elements of NSGA II. The methodology is illustrated by a typical example.

Streszczenie. W artykule prezentowana jest optymalizacja kształtu urządzenia do indukowania grzania wstępnego stalowych obiektów w celu otrzymania najlepszego działania. Celem jest maksymalizacja ciepła dostarczanego do miejsca w obiekcie, które zostanie poddane grzaniu wiązką laserową, przy jednoczesnej minimalizacji ciepła dostarczanego wszędzie indziej. Zagadnienie proste (silnie sprzężona analiza pola magnetycznego i pola temperaturowego w systemie) rozwiązane zostało metodą elementów skończonych. Zagadnienie odwrotne rozwiązywane jest przy użyciu specjalnego algorytmu genetycznego z pewnymi elementami NSGA II. Metodyka została zilustrowana typowym przykładem. (Optymalizacja specjalnego induktora dla indukcji grzania wstępnego)

Introduction

Presently, induction pre-heating of metals belongs to prospective technologies for their surfacing (such as laser welding or hardening), see, for example, [1–4]. Its purpose is to suppress unacceptably high temperature gradients in the surface layers of heated material irradiated later by a laser beam and avoid problems connected with subsequent excessive local mechanical strains and stresses of the thermal origin [5].

The considered pre-heater consists of a long copper inductor placed in a ferrite shell serving as a flux concentrator (ferrite is chosen because of its poor electric conductivity, low induced currents and Joule losses). The bottom part of the inductor is covered by a thin layer of thermal insulation in order to prevent the ferrite part from excessive heating by convection and radiation that would lead to deterioration of the ferrite parameters. The transverse cut through the inductor is depicted in Fig. 1. It moves at a prescribed velocity v above the surface of the heated body, in the direction perpendicular to the picture plane. Thus, the material is first pre-heated by the inductor and only after it is heated by the laser beam. The variations of the temperature at the exposed spots are then not as fast as in the case of the single laser.

Fig. 1. Basic arrangement of inductor

The paper deals with the shape optimization of a cylindrical pre-heater whose goal is to secure its highest efficiency (which means the highest heat losses in the domain to be preheated and minimum heat losses elsewhere). Selected dimensions of the inductor are, however, subject to specific technological constraints.

Formulation of the technical problem

The goal of this paper is to optimize the inductor. The original dimensions of its cut (in mm) are indicated in Fig. 2. About a half of them are fixed, but several others denoted by letters $a, ..., g$ can change within the prescribed ranges.

The principal results of computations will be the optimized dimensions $a, ..., g$ satisfying the requirements on the distribution of delivered heat. Other results are the profiles of magnetic and temperature fields in the system with the optimized inductor and also the most important profiles of the temperature.

Fig. 2. Original dimensions of the inductor

Mathematical model

From the mathematical viewpoint, the task represents a non-linear inverse problem and particular steps of its solution are iterative computations of magnetic and temperature fields in the system and a multi-criteria optimization procedure for obtaining the best possible dimensions of the inductor. Its solution consists of the following iterative steps:
1. Proposal of two objective functions quantifying the amounts of heat produced by induction in both domains of interest.
2. Proposal of the first genetic population.
3. Computation of both functionals for the individuals and creation of the Pareto diagram.
4. If the Pareto front is unacceptably different from the same front obtained in the previous step, proposal of a new population and return to step 3.
5. End of computations.

Details concerning the above steps are discussed in the following steps:

1. The objective functions were the total heat losses Q_1 in the domain to be preheated (the region below the inductor, see Fig. 1) and total heat losses outside this domain Q_2. After optimization, Q_1 should reach its maximum while Q_2 should reach its minimum. Determination of Q_1 and Q_2 will be shown later.

2. The optimization process was based on using a specific in-house genetic algorithm. The first population consisted of vectors containing estimated values of dimensions that may vary.

3. For every individual of the population we determine the values of Q_1 and Q_2. This step is rather long and first we will describe its individual parts.

• Coupled solution of the magnetic and temperature fields in the system. This task is solved in the hard-coupled formulation in order to respect the time dependences of all important material parameters. The *magnetic field* is described by the equation for the magnetic vector potential A [6]

$$(1) \quad \mathrm{curl}\left(\frac{1}{\mu}\mathrm{curl}\,A\right) + \gamma\frac{\partial A}{\partial t} = J_{\text{ext}} ,$$

where μ is the magnetic permeability, γ denotes the electric conductivity and J_{ext} stands for the vector of the external harmonic current density in the field coil. But solution to (1) is, in this particular case, practically unfeasible. The reason consists in a deep disproportion between the frequency f (usually thousands Hz) of the field current I_{ext} and time of heating t_{H} (several seconds). That is why the model was somewhat simplified using the assumption that the magnetic field is harmonic. In such a case it can be described by the Helmholtz equation for the phasor $\underline{A}$ of the magnetic vector potential A [7]

$$(2) \quad \mathrm{curl\,curl}\,\underline{A} + \mathrm{j}\cdot\omega\gamma\mu\underline{A} = \mu\underline{J}_{\text{ext}} .$$

Here, ω denotes the angular frequency ($\omega = 2\pi f$). But the magnetic permeability μ of ferromagnetic parts is supposed not to be a constant everywhere; in every cell of the discretization mesh it is assigned to the local value of the magnetic flux density. Its computation is, in such a case, based on an appropriate iterative procedure. The conditions along the axis of the system and artificial boundary placed at a sufficient distance from it are of the Dirichlet type ($\underline{A} = \mathbf{0}$).

The *temperature field* T in the clamping head is described by the heat transfer equation [8]

$$(3) \quad \mathrm{div}\left(\lambda\cdot\mathrm{grad}\,T\right) = \rho c_{\text{p}}\cdot\frac{\partial T}{\partial t} - w ,$$

where λ is the thermal conductivity, ρ denotes the mass density and c_{p} stands for the specific heat (all of these parameters are generally temperature-dependent functions). Finally, symbol w denotes the time average internal volumetric sources of heat that generally consist of the volumetric Joule losses w_{J} (due to eddy currents) and magnetization losses w_{m}. Thus, we can write

$$(4) \quad w = w_{\text{J}} + w_{\text{m}} ,$$

where

$$(5) \quad w_{\text{J}} = \frac{\left|\underline{J}_{\text{eddy}}\right|^2}{\gamma} , \quad \underline{J}_{\text{eddy}} = -\mathrm{j}\cdot\omega\gamma\underline{A} ,$$

while w_{m} are determined from the known measured loss dependence $w_{\text{m}} = w_{\text{m}}\left(\left|\underline{B}\right|\right)$ for the material used (magnetic flux density B in every element of the mesh is in this model also harmonic), or from the Steinmetz formula. In many cases, however, the magnetization losses are neglected as their value is very small with respect to the Joule losses. The boundary conditions take into account convection and radiation and may be written in the form

$$(7) \quad -\lambda\frac{\partial T_{\text{S}}}{\partial n} = \alpha\left(T_{\text{S}} - T_{\text{ext}}\right) + \sigma C\left(T_{\text{S}}^4 - T_{\text{r}}^4\right) .$$

In the above equation, α denotes the coefficient of convective heat transfer, T_{S} stands for the surface temperature, T_{ext} is the temperature of ambient medium and n represents the direction of the outward normal to the surface S of the body at a given point. Symbol σ expresses the Stefan--Boltzmann constant, C is the coefficient of emissivity that may also include the configuration factor and influence of the multiple reflections and, finally, T_{r} stands for the temperature of surface to which heat from the system is radiated.

• The functionals Q_1 and Q_2 are given by the relations

$$(8) \quad Q_1 = \int_0^{t_{\text{H}}}\int_{V_1}\left(w\,\mathrm{d}V\right)\mathrm{d}t , \quad Q_2 = \int_0^{t_{\text{H}}}\int_{V_2}\left(w\,\mathrm{d}V\right)\mathrm{d}t ,$$

where V_1 is the volume of the domain with the heat losses that are to be maximized, while V_2 is the remaining volume of the body where the heat losses should be as low as possible. Both functionals are calculated for every individual from the population and drawn into a corresponding Pareto diagram.

Evaluation of the Pareto front in the diagram. If the position of this front differs from the front obtained in the previous population by more than a prescribed tolerance, a new population is created, where the individuals are generated from the previous individuals by mutation and crossover. Thus, an iterative process is started up that is stopped at the moment when the above difference is acceptable.

Numerical solution

Both the field computations (in the monolithic formulation respecting all non-linearities and temperature dependences of the material parameters) and optimization were performed using our own code Agros2D.

This application [9] cooperating with the library Hermes [10] is based on a fully adaptive higher-order finite element method [11]. Both these codes written in C++ are intended for the numerical solution of systems of generally non-linear and non-stationary second-order partial differential equations (PDEs) and their principal purpose is to model complex physical phenomena. They are freely distributable under the GNU General Public License. We can mention some of their unique features such as:

• Solution of a system of PDEs may be carried out in both weakly coupled and hard-coupled formulations. In the latter case, the resultant numerical scheme is characterized by just one stiffness matrix.

• There are three kinds of the adaptive algorithms implemented in the code. Except for more common *h*-adaptivity and *p*-adaptivity, also the most sophisticated *hp*-adaptivity may be used. The orders of the corresponding polynomials may reach 10.

• Each of the mapped physical fields can be solved on a quite different mesh. For example, the temperature field is often highly smooth, so that it is not necessary to solve it on

an unnecessarily dense mesh (such as in case of the magnetic fields). As far as the task is non-stationary, the meshes evolve in time according to the results obtained in the previous step.

- The codes can work with the hanging nodes of any level, which leads to a substantial reduction of the degrees of freedom (DOFs).
- Besides the classic triangles, the codes are able to mix even quadrilateral and curved elements. The curved elements are very advantageous for accurate modelling curvilinear boundaries and interfaces.
- The application also contains a powerful optimization module based on several kinds of genetic algorithms and conjugate gradients.

Illustrative example

The goal of the example is to illustrate the process of shape optimization of a typical inductor used for this purpose in one of the Czech companies.

The dimensions of this inductor are shown in Fig. 1. Its body is made of ferrite of the following parameters: relative permeability $\mu_r = 40$ and electric conductivity $\gamma = 1$ S/m. The starting dimensions are: $a = 10$ mm, $b = 38$ mm, $c = 5$ mm, $d = 19$ mm, $e = 45$ mm, $f = 4$ mm, and $g = 1$ mm. The field current density $J_{ext} = 10^6$ A/m^2, and its frequency $f = 15$ kHz.

The heated body is a massive plate made of carbon steel CSN 12040. Its nonlinear characteristics are depicted in the following figures. Figure 3 shows its saturation curve at the room temperature.
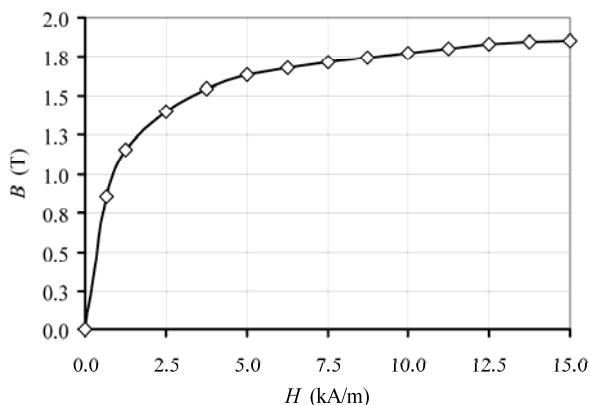
Fig. 3. Saturation curve of steel CSN 12040 at the room temperature

The magnetic permeability $\mu_r = \mu_r(B,T)$ depends also on the temperature. This dependence is assumed to have a form $\mu_r(B,T) = \mu_r(B,T_r) \cdot \psi(T)$, where T_r is the room temperature and $\psi(T)$ is a suitable function of the temperature. We suppose that

(9)   for $T_r \leq T \leq T_C$ $\psi(T) = a - bT^2$,

        for $T_C \leq T$ $\psi(T) = \dfrac{1}{\mu_r(B,T_r)}$.

Here

(10) $a = \dfrac{\mu_r(B,T_r)T_C^2 - T_r^2}{\mu_r(B,T_r)(T_C^2 - T_r^2)}$, $b = \dfrac{\mu_r(B,T_r) - 1}{\mu_r(B,T_r)(T_C^2 - T_r^2)}$,

symbol T_C denoting the Curie temperature (for steel CSN 12040 its value is approximately 760 °C).

For the sane steel, Fig. 4 shows the temperature dependence of its electric conductivity, Fig. 5. depicts an analogous dependence of its thermal conductivity and Fig. 6 contains the graph of its specific heat capacity.

The optimization process has the following technological constraints: $a \subset \langle 5 - 20 \rangle$ mm, $b \subset \langle 0 - 39 \rangle$ mm, $c \subset \langle 5 - 20 \rangle$ mm, $d \subset \langle 5 - 20 \rangle$ mm, $e \subset \langle 20 - 60 \rangle$ mm, $f \subset \langle 1 - 10 \rangle$ mm, and $g \subset \langle 1 - 10 \rangle$ mm.

The velocity of the inductor $v = 3$ mm/s, the initial temperature $T_0 = 20$ °C, and the generalized coefficient of the heat convection (respecting also the radiation) $\alpha = 15$ W/m^{2}K. The computations are performed for the steady state of the process; this means that the temperature field does not explicitly change with time, but only with the position of the inductor.
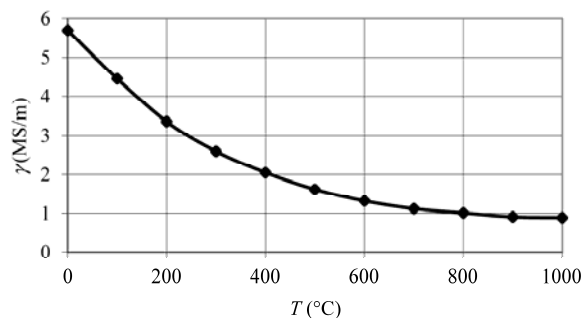

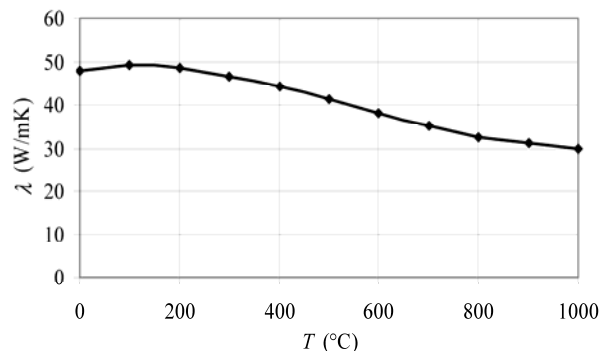Fig. 4. Electric conductivity of steel CSN 12040 vs temperature

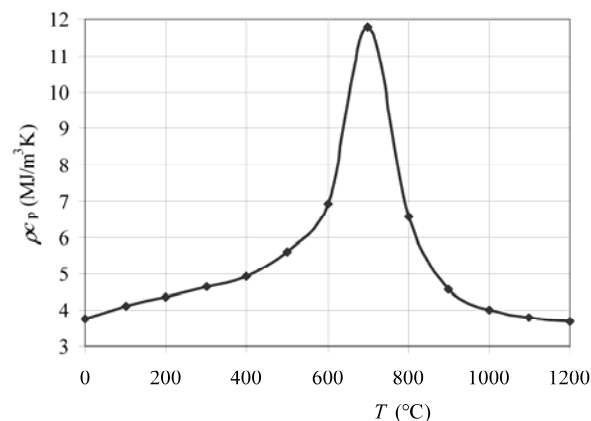Fig. 5. Thermal conductivity of steel CSN 12040 vs temperature

Fig. 6. Specific heat capacity of steel CSN 12040 vs temperature

In the optimization process, every generation was formed by 50 individuals and during one generation just about one third of the original population was preserved, while another third were generated by crossover. The ancestors for the crossover were selected according to their position with respect to the Pareto front. The remaining third of the population were obtained by mutation. In all generations, the coupled problem of induction heating was solved and both objective functions were evaluated. The

process was finished after 55 generations, when the Pareto front practically stopped changing.

Figure 7 shows the evolution of the optimization process with the final shape of the Pareto front (in the next iterations the Pareto front did not change any longer).

After a detailed evaluation of the results we selected the optimized dimensions of the inductor: $a = 5$ mm, $b = 30$ mm, $c = 10$ mm, $d = 10$ mm, $e = 41$ mm $f = 4.5$ mm, and $g = 7$ mm. For comparison, the original and optimized shapes of the inductor (together with the distribution of magnetic flux density) are in Fig. 8.
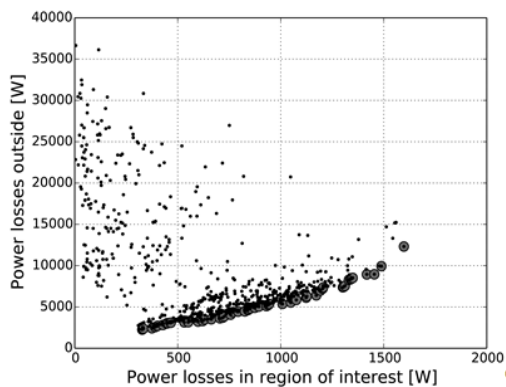
Fig. 7. Evolution of optimization process and final Pareto front after 55 generations marked by larger grey circles (left) and distribution of the surface temperatures along the longitudinal axis of the domain with required maximum heat losses (right)
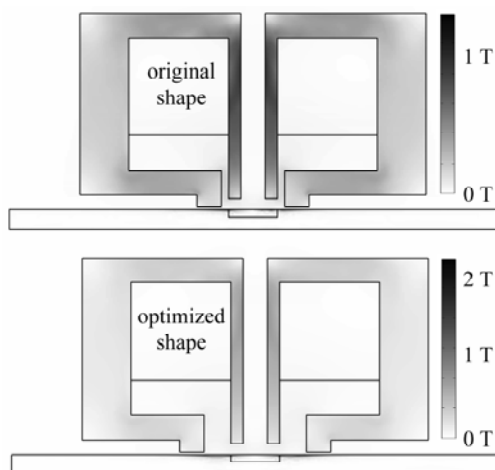
Fig. 8. Original (up) and optimized (bottom) shapes of the inductor, together with the distribution of magnetic flux density
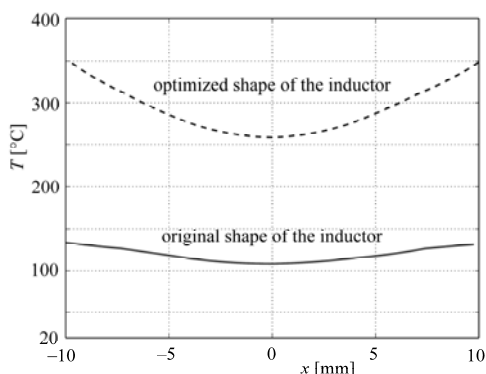
Fig. 9. Surface temperature along the longitudinal axis of the domain with required heat losses (see Fig. 1)

A very important result is the profile of the surface temperature along the longitudinal axis of the domain (see Fig. 1) with the required maximized heat losses. These profiles are depicted in Fig. 9 and it is obvious that in the case of the optimized inductor the surface temperature is more than two times higher.

Conclusion
The paper presents the shape optimization of a pre-heating inductor with the aim to maximize the heat losses in a specific domain of the heated body, while in its exterior the same losses are minimized. From the mathematical viewpoint, the task represents an inverse coupled problem. The coupled problem of induction heating is solved by our own code in the monolithic formulation, the optimization being carried out using an in-house genetic algorithm developed by the authors.
Next work in the field will be aimed at the modelling of cooperation of the optimized pre-heater and laser beam during the process of the combined heating and experimental verification of the results. Attention will also be paid to the acceleration of the computational algorithms. Last but at least, the influence of frequency on the shape optimization will also be investigated.

REFERENCES
[1] P. Mackwood, R. C. Crafer: Thermal modelling of laser welding and related processes: a literature review. Optics & Laser Technology 37 (2), pp. 99–115 (2005).
[2] M. F. Ashby, K. A. Easterling: The transformation hardening of steel surfaces by laser beams: I. Hypo-eutectoid steels. Acta Metallurgica 32 (11), pp. 1935–1948 (1984).
[3] A. K. Nath, A. Gupta, F. Benny: Theoretical and experimental study on laser surface hardening by repetitive laser pulses. Surface and Coatings Technology 206 (8–9), pp. 2602–2615 (2012).
[4] S. Skvarenina, Y. C. Shin: Predictive modeling and experimental results for laser hardening of AISI 1536 steel with complex geometric features by a high power diode laser. Surface and Coatings Technology 201 (6), pp. 2256–2269 (2006).
[5] S. S. Akhtar, B. S. Yilbas: Laser treatment of steel surfaces: Numerical and experimental investigations of temperature and stress fields. Comprehensive Materials Processing, Elsevier, pp. 25–46 (2014).
[6] M. Kuczmann, A. Iványi: The finite element method in magnetics. Akadémiai Kiadó, Budapest (2008).
[7] J. A. Stratton: Electromagnetic theory. Wiley-IEEE Press, New York (2007).
[8] J. P. Holman: Heat transfer, McGraw-Hill, New York (2002).
[9] P. Karban and others: C++ application for the solution of PDEs. Available: http://agros2d.org.
[10] P. Solin and others: Hermes - Higher-order modular finite element system (User's guide). Available: http://hpfem.org.
[11] P. Solin, K. Segeth, I. Dolezel: Higher-order finite element methods, CRC Press, Boca Raton, FL, USA (2003).

Authors: *Ing. David Pánek, Ph.D., Ing. Václav Kotlan, Ph.D., University of West Bohemia, Faculty of Electrical Engineering, Univerzitní 26, 306 14 Plzeň, Czech Republic, {panek50, vkotlan}@kte.zcu.cz. Prof. Ing. Ivo Doležel, CSc., Academy of Sciences of the Czech Republic, Institute of Thermomechanics, Dolejškova 5, 182 00 Praha 8, Czech Republic, dolezel@it.cas.cz.*